The FEBS Journal

FEBS PRESS science publishing by scientists

EDITOR'S CHOICE

Hsp90α regulates ATM and NBN functions in sensing and repair of DNA double-strand breaks

Rosa Pennisi[1], Antonio Antoccia[1,2], Stefano Leone[1], Paolo Ascenzi[1] and Alessandra di Masi[1,2]

1 Department of Sciences, Roma Tre University, Roma, Italy
2 Istituto Nazionale Biostrutture e Biosistemi, Roma, Italy

Keywords
17-AAG; ATM; DNA damage response; DNA double-strand break; H2AX; Hsp90α; ionizing radiation; NBN

Correspondence
A. di Masi, Department of Sciences, Roma Tre University, Viale Guglielmo Marconi 446, I-00146 Roma, Italy
Fax: +39-06-57336321
Tel: +39-06-57336363
E-mail: alessandra.dimasi@uniroma3.it

(Received 20 December 2016, revised 11 May 2017, accepted 15 June 2017)

doi:10.1111/febs.14145

[Correction note: The same panel was inadvertently shown for all four flow cytometric analyses in figure 7A and 7C. A Corrigendum, showing the corrected figure 7, was published in Wiley Online Library on 12 November 2017 and it can be found at https://doi.org/10.1111/febs.14298]

The molecular chaperone heat shock protein 90 (Hsp90α) regulates cell proteostasis and mitigates the harmful effects of endogenous and exogenous stressors on the proteome. Indeed, the inhibition of Hsp90α ATPase activity affects the cellular response to ionizing radiation (IR). Although the interplay between Hsp90α and several DNA damage response (DDR) proteins has been reported, its role in the DDR is still unclear. Here, we show that ataxia-telangiectasia-mutated kinase (ATM) and nibrin (NBN), but not 53BP1, RAD50, and MRE11, are Hsp90α clients as the Hsp90α inhibitor 17-(allylamino)-17-demethoxygeldanamycin (17-AAG) induces ATM and NBN polyubiquitination and proteosomal degradation in normal fibroblasts and lymphoblastoid cell lines. Hsp90α-ATM and Hsp90α-NBN complexes are present in unstressed and irradiated cells, allowing the maintenance of ATM and NBN stability that is required for the MRE11/RAD50/NBN complex-dependent ATM activation and the ATM-dependent phosphorylation of both NBN and Hsp90α in response to IR-induced DNA double-strand breaks (DSBs). Hsp90α forms a complex also with ph-Ser1981-ATM following IR. Upon phosphorylation, NBN dissociates from Hsp90α and translocates at the DSBs, while phThr5/7-Hsp90α is not recruited at the damaged sites. The inhibition of Hsp90α affects nuclear localization of MRE11 and RAD50, impairs DDR signaling (e.g., BRCA1 and CHK2 phosphorylation), and slows down DSBs repair. Hsp90α inhibition does not affect DNA-dependent protein kinase (DNA-PK) activity, which possibly phosphorylates Hsp90α and H2AX after IR. Notably, Hsp90α inhibition causes H2AX phosphorylation in proliferating cells, this possibly indicating replication stress events. Overall, present data shed light on the regulatory role of Hsp90α on the DDR, controlling ATM and NBN stability and influencing the DSBs signaling and repair.

Introduction

Cells respond to the spontaneous and induced DNA damage through the activation of a complex DNA damage response (DDR) pathway that includes cell cycle arrest, transcriptional and post-translational

Abbreviations
17-AAG, 17-(allylamino)-17-demethoxygeldanamycin; ATM, ataxia-telangiectasia-mutated kinase; ATR, ataxia-telangiectasia and Rad3-related kinase; co-IP, co-immunoprecipitation; DDR, DNA damage response; DNA-PK, DNA-dependent protein kinase; DSB, DNA double-strand break; HER2, human epidermal growth factor receptor 2; HR, homologous recombination; Hsp90α, heat shock protein 90α; IR, ionizing radiation; LCL, lymphoblastoid cell lines; MRN, MRE11/RAD50/NBN complex; NBN, nibrin; NBS, Nijmegen breakage syndrome; NHEJ, nonhomologous end-joining; PIKK, phosphatidylinositol-3-kinase protein kinase-like; poly-Ub, polyubiquitination; PTMs, post-translational modifications.

activation of genes involved in the DNA repair, and, eventually, in the induction of apoptosis [1–3]. The DNA double-strand break (DSB) represents one of the most harmful DNA lesion and DSBs repair requires the expression and activity of damage sensors like the phosphatidylinositol-3-kinase protein kinase-like (PIKK) family members. This family includes the ataxia-telangiectasia-mutated (ATM) kinase, the ataxia-telangiectasia and Rad3-related (ATR) kinase, and the DNA-dependent protein kinase (DNA-PK) [4,5]. While ATM and DNA-PK are activated in response to ionizing radiation (IR) [6], ATR is activated by UV-induced replication fork stalling [7,8]. ATM signaling is a finely tuned mechanism that regulates the DSBs response [9,10]. Indeed, ATM phosphorylates more than 700 target proteins in human cells, including DNA damage sensor and repair proteins (e.g., 53BP1 [11], BRCA1 [12], H2AX [13], MDC1 [14], MRE11 [15], nibrin (also known as NBN) [16], and RAD50 [17]), cell cycle regulators (e.g., p53 [18] and RAD9A [19]), and kinases (e.g., CHK2 [20], DNA-PK [21], and AKT [22]).

The MRE11/RAD50/NBN (MRN) trimer is one of the first complexes recruited to the DSB sites where it bridges the DSB ends and contributes to the recruitment of ATM molecules through a direct interaction with the C terminus of NBN [23]. The ATM–NBN interaction and the ATM-dependent phosphorylation of NBN [16,24,25] are pivotal for ATM and NBN recruitment and retention at the DSB sites [26,27]. Furthermore, the MRN complex is required for the DSBs repair that can take place by either the nonhomologous end-joining (NHEJ) or the homologous recombination (HR) repair mechanisms [23,28]. This implies the existence of an important and finely regulated crosstalk between ATM and the MRN complex in order to properly respond, signal, and repair the DSBs [5].

Overall, the efficacy of the DDR is influenced by the nuclear levels of the DNA repair proteins, which are regulated by balancing between protein synthesis and degradation, and by the control of the nuclear protein import and export [29]. Molecular chaperones play a key role in protein homeostasis (also termed proteostasis), regulate protein folding and functions, and mitigate the harmful effects of endogenous and exogenous stressors on the proteome [30–33]. Heat shock protein 90α (Hsp90α) represents a proteostasis hub that coordinates both protein assembly and degradation. In particular, Hsp90α is not required for the *de novo* protein folding, but rather facilitates the final maturation of proteins to allow their interaction with binding partners. This highlights the pivotal role of Hsp90α in orchestrating the spatial and temporal order of protein–protein interactions [33–35] and in regulating several signaling pathways in eukaryotic cells such as the DDR (see refs in [29]). Hsp90α regulates the stability of several DDR proteins (e.g., ATR, BRCA1, BRCA2, CHK1, the MRN complex, and RAD51) [29], and, in response to DNA damage, it is phosphorylated by PIKK family members at the Thr5 and Thr7 residues (i.e., DNA-PK and ATM, depending on the DNA damage inducer) [36].

Here, we show that ATM and NBN are clients of Hsp90α and that Hsp90α-ATM and Hsp90α-NBN complexes are present both in unstressed and irradiated cells. This allows the maintenance of ATM and NBN stability that is required for MRN-dependent ATM activation and ATM-dependent phosphorylation of both NBN and Hsp90α in response to IR-induced DNA damage. However, while phosphorylated NBN dissociates from Hsp90α and translocates at the DSBs, Hsp90α phosphorylated at the Thr5 and Thr7 residues partially colocalizes with γ-H2AX at the DSB sites. Furthermore, the inhibition of Hsp90α ATPase activity affects the nuclear localization of MRE11 and RAD50, impairs the activation of the DDR signaling pathway, and slows down the DSBs repair. Overall, the present data shed light on the regulatory role of Hsp90α in the DDR, by controlling ATM and NBN stability and influencing the overall DSBs signaling and repair.

Results

ATM and NBN are Hsp90α clients

Although Hsp90α has been reported to facilitate the ATM–NBN interaction [37], the regulatory role of Hsp90α in the very early phases of DSBs sensing is unclear. To pursue this issue, the effect of the 17-(allylamino)-17-demethoxygeldanamycin (17-AAG), an inhibitor of the ATPase activity of Hsp90α [29,38], on the expression of ATM, 53BP1, RAD50, MRE11, and NBN was evaluated in human MRC5-SV40 immortalized fibroblasts and in human normal lymphoblastoid cell lines (LCL).

In both MRC5-SV40 and LCL the dose-dependent reduction in ATM and NBN levels was observed after 8 h of treatment with 17-AAG (Fig. 1A). Time-dependent experiments indicated that the treatment with 1 μM 17-AAG caused the decrease in ATM and NBN levels over time, with a significant reduction in their levels starting at 8 h from the treatment, both in MRC5-SV40 and LCL (Fig. 1B). Of note, the inhibition of the ATPase activity of Hsp90α by 17-AAG did not alter the expression of either 53BP1 or of the other two members of the MRN complex, that are RAD50

and MRE11 (Fig. 1A). A dose- and time-dependent evaluation of ATM and NBN levels has been performed also using radicicol, a structurally unrelated Hsp90α inhibitor. While the treatment of MRC5-SV40 cells with 1 μM of radicicol did not affect ATM and NBN expression (data not shown), cell exposure to 2 μM radicicol resulted in the almost complete degradation of ATM and NBN within 4 h (Fig. 1C).

The inhibition of Hsp90α induces the proteasomal degradation of its clients [39], therefore we evaluated the role of the proteasome on the 17-AAG-induced degradation of ATM and NBN. MRC5-SV40 cells were pretreated for 2 h with 1 nM MG-132, a potent proteasome inhibitor, and then exposed for further 14 h to 1 μM 17-AAG. We observed that MG-132 induced an increase in the total amount of polyubiquitinated (poly-Ub) proteins, indicating the efficient proteasome inhibition. When cells were treated with MG-132 and then exposed to 17-AAG, the degradation of ATM and NBN was partially reversed, suggesting that the inhibition of Hsp90α activity induces the proteasomal degradation of ATM and NBN (Fig. 1D).

Since Hsp90α inhibition may affect overall cell proliferation [40], we evaluated whether ATM and NBN degradation may be due to 17-AAG-induced cytotoxic effects. The 3-(4,5-dimethylthiazol-2-yl)-2,5-diphenyltetrazolium bromide (MTT) assay showed that the exposure to increasing doses of 17-AAG caused a mild

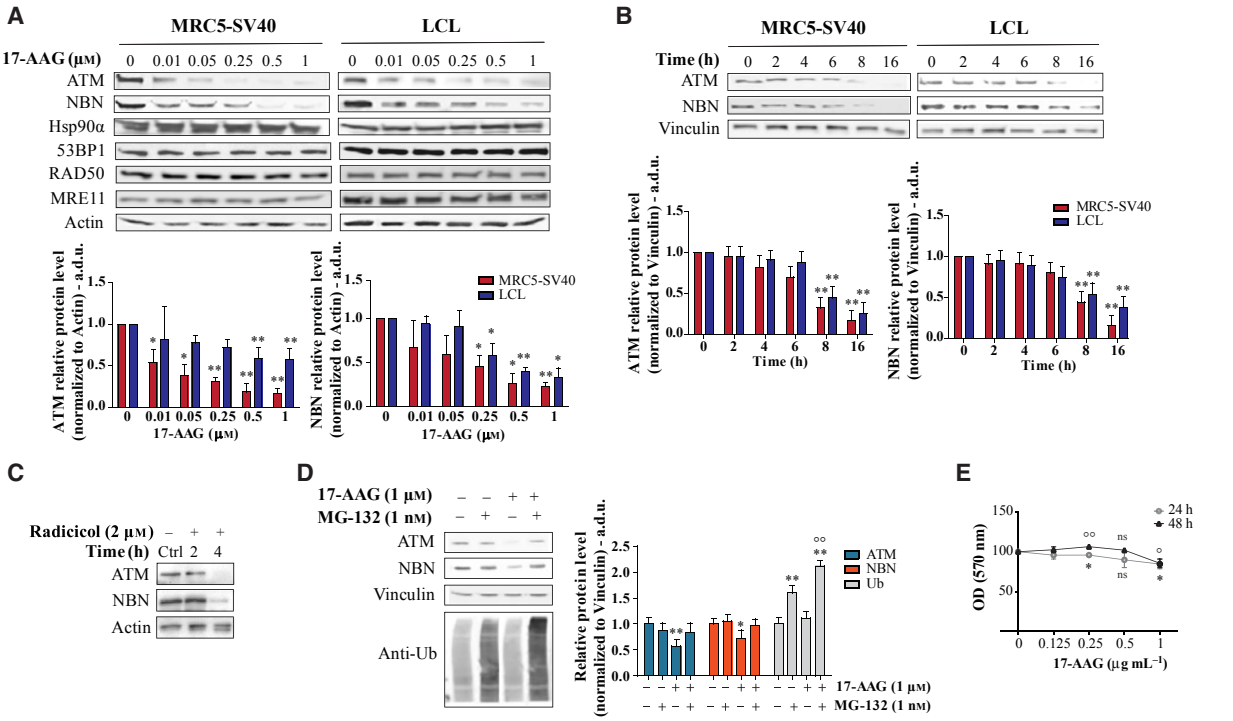

Fig. 1. The inhibition of the Hsp90α ATPase activity by 17-AAG induces the dose- and time-dependent degradation of ATM and NBN in MRC5-SV40 and LCL cells. (A) Dose-dependent experiments and relative densitometric analyses performed in cells treated with 0, 0.01, 0.05, 0.25, 0.5, and 1 μM 17-AAG for 8 h. (B) Time-dependent experiments performed in cells treated with 1 μM 17-AAG for 2, 4, 6, 8, and 16 h. Immunoblots were performed using anti-ATM, anti-NBN, anti-Hsp90α, anti-53BP1, anti-RAD50, and anti-MRE11 antibodies; actin and vinculin were used as loading controls. Graphs represent the fold induction of ATM and NBN levels in treated versus untreated cells, normalized to actin or vinculin ± SD (Student's *t*-test, $*P < 0.05$ and $**P < 0.01$, with respect to relative controls; a.d.u., arbitrary densitometric unit), derived from three independent experiments. (C) Time-dependent experiments performed in MRC5-SV40 cells treated with 2 μM radicicol for 2 and 4 h. Immunoblots were performed using anti-ATM and anti-NBN antibodies; actin was used as loading control. (D) Western blot analysis of MRC5-SV40 cells pretreated for 2 h with 1 nM of the proteasome inhibitor MG-132 and then exposed to 1 μM 17-AAG for further 14 h. Immunoblots were performed using anti-ATM, anti-NBN, and anti-Ub antibodies. The graph represents the fold induction of ATM and NBN levels in treated versus untreated cells, normalized to vinculin ± SD (Student's *t*-test, $*P < 0.05$ and $**P < 0.01$, with respect to relative controls; $°°P < 0.01$ with respect to MG-132-treated cells; a.d.u., arbitrary densitometric unit), derived from two independent experiments. (E) MRC5-SV40 cells were treated for 24 and 48 h with 0.125, 0.250, 0.5, and 1 μM 17-AAG and cytotoxic effects were determined by MTT assay. The graph represents the percentage of viable cells normalized to solvent (DMSO)-treated cells ± SD (Student's *t*-test, $*P < 0.05$ and $**P < 0.01$, with respect to DMSO-treated cells fixed at 24 h; $°P < 0.05$ and $°°P < 0.01$, with respect to DMSO-treated cells fixed at 48 h), derived from three replicates.

cytotoxicity in MRC5-SV40 cells, with a 85.5% of cell survival after 24 and 48 h exposure to 1 μM 17-AAG (Fig. 1E). This indicates that the 17-AAG-dependent degradation of ATM and NBN after 8 h of exposure to the drug is directly associated with the inhibition of Hsp90α ATPase activity rather than caused by 17-AAG-induced cytotoxic effects.

Hsp90α interacts with ATM and NBN both in unstressed cells and following IR-induced DNA damage

Previous data from our lab demonstrated that Hsp90α and NBN interact both in unstressed condition and following IR-induced damage in HEK293 cells [41]. To clarify the role of Hsp90α in the interaction between ATM and NBN during the DDR, co-immunoprecipitation (IP) experiments were performed in cells exposed to 4 Gy of X-rays and harvested after 0.5, 3, and 6 h.

The anti-Hsp90α antibody coprecipitated ATM and NBN in unstressed MRC5-SV40 cells, the level of Hsp90α-ATM and Hsp90α-NBN complexes increasing following IR. In particular, while Hsp90α-ATM levels significantly increased at 0.5 and 3 h from IR ($P < 0.05$) and returned to basal levels after 6 h from IR (Fig. 2A,B), Hsp90α-NBN levels reached a peak at 0.5 h from IR ($P < 0.001$) and returned to basal levels after 3 h from DSBs induction (Fig. 2A,B). Of note, Hsp90α interacted also with phSer1981-ATM, but not with phSer343-NBN, the complex reaching a peak at 0.5 h from IR and persisting after 3 and 6 h from IR ($P < 0.001$ with respect to untreated cells; Fig. 2A,C). As expected [42], in the whole-cell extracts (input) the total levels of ATM and NBN were unchanged before and after irradiation, whereas phSer1981-ATM levels increased after 0.5 h from IR and persisted at 3 and 6 h from IR, and phSer343-NBN levels progressively increased after 0.5, 3, and 6 h from IR (Fig. 2A). The total levels of Hsp90α and phThr5/7-Hsp90α did not change following IR compared to basal levels (Fig. 2A).

The Hsp90α–NBN interaction requires the integrity of the NBN protein, as suggested by the lack of interaction in cells established from a Nijmegen breakage syndrome (NBS) patient (here named $NBN^{657del5}$; Fig. 2D,E), homozygous for the 657del5 mutation that causes the expression of two truncated isoforms partially retaining the NBN full-length functions [42–44]. The interaction between Hsp90α and NBN was also evaluated in the NBS-derived cell line ectopically expressing an NBN protein carrying the point mutation Ser343Ala (here named 343S), which prevents the ATM-dependent phosphorylation of the Ser343 residue of NBN following IR [16]. As shown in Fig. 2D, E, the level of the Hsp90α-NBN complex increased by 2.8-folds ($P < 0.05$) in 343S-irradiated cells compared to control. This suggests that in normal cells the interaction between Hsp90α and NBN is reduced following the ATM-dependent phosphorylation of the Ser343 residue of NBN following IR.

The reverse co-IP experiment performed with the anti-NBN antibody confirmed the increase in NBN total levels and in the ATM-NBN complex levels after 0.5 h from IR compared to the relative controls, and the existence of an Hsp90α-NBN complex in untreated cells, whose level increased after 0.5 h from IR (Fig. 3A). Although both MRE11 and RAD50 coprecipitated with NBN in untreated cells and even more after IR (Fig. 3A), neither MRE11 nor RAD50 coprecipitated with Hsp90α, although both proteins were detected in the input of untreated and irradiated cells (Fig. 2A).

The interaction between Hsp90α and NBN is regulated by ATM kinase activity

To prove the hypothesis that the interaction between Hsp90α and NBN is regulated by the ATM kinase activity, we evaluated the levels of the Hsp90α-NBN complex in the absence of ATM or by inhibiting its kinase activity. The increase of the Hsp90α-NBN complex levels was detected following IR in cells established from an ataxia-telangiectasia patient (here named $ATM^{-/-}$; 1.8-fold, $P < 0.05$; Fig. 2D,E), in ATM-silenced MRC5-SV40 fibroblasts (Fig. 3B), and in MRC5-SV40 cells treated with the ATM kinase inhibitor KU60019, compared to their relative controls (Fig. 3C).

The co-IP experiment performed using the anti-ATM antibody resulted in the coprecipitation of NBN, Hsp90α, and of its phosphorylated form in untreated cells, the levels of all these complexes increasing after 0.5 h from IR (Fig. 3D). Of note, ATM phosphoryated Hsp90α at the Thr5/7 residues, as demonstrated by the reduction in the phThr5/7-Hsp90α levels in MRC5-SV40 cells treated with the KU60019 ATM inhibitor (Fig. 3E) [45].

The phosphorylated Hsp90α is not recruited at the DSBs following IR

γ-H2AX and 53BP1 are well-known markers of the DSBs that mediate the accumulation of various signaling and repair proteins to the damaged sites to form the so-called IR-induced foci (IRIF) [46,47]. Although

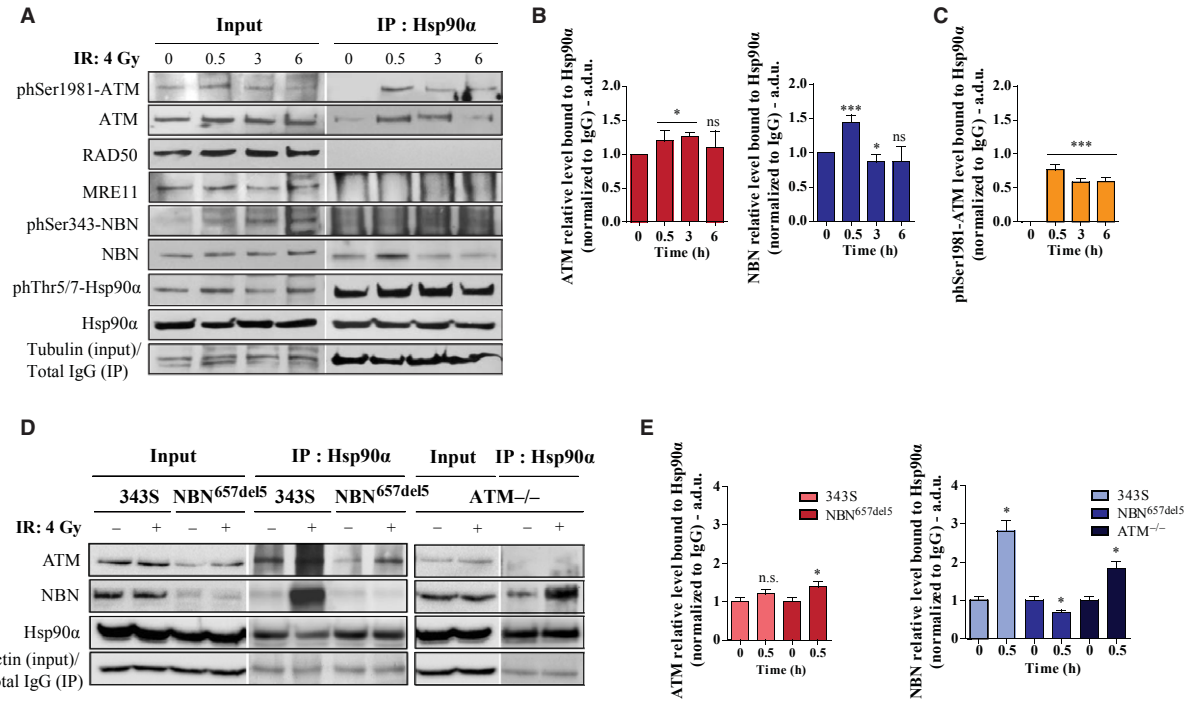

Fig. 2. Hsp90α interacts with ATM and NBN in unstressed cells and in response to IR-induced DNA damage. (A) MRC5-SV40 cells were irradiated with 4 Gy of X-rays and harvested after 0.5, 3, and 6 h. Five hundred micrograms of total protein extracts were immunoprecipitated with anti-Hsp90α antibody, and 10 μg of total protein lysate were loaded as input. Membranes were probed with anti-phSer1981-ATM, anti-ATM, anti-phSer343-NBN, anti-NBN, anti-phThr5/7-Hsp90α, and anti-Hsp90α, anti-RAD50, and anti-MRE11 antibodies. (B) Graphs represent the fold induction of ATM and NBN levels immunoprecipitated with Hsp90α in treated versus untreated cells, normalized to IgG ± SD (Student's *t*-test, $*P < 0.05$ and $***P < 0.001$, with respect to the relative control; a.d.u., arbitrary densitometric unit), derived from two independent experiments. (C) Graphs represent the levels of phSer1981-ATM co-immunoprecipitated with Hsp90α in untreated and irradiated cells, normalized to IgG ± SD (Student's *t*-test, $***P < 0.001$ with respect to untreated cells; a.d.u., arbitrary densitometric unit) derived from two independent experiments. (D) The 343S, NBN^{657del5}, and ATM$^{-/-}$ cells were irradiated with 4 Gy of X-rays and fixed after 0.5 h. Five hundred micrograms of total protein extracts were immunoprecipitated with anti-Hsp90α antibody, and 10 μg of total protein lysate were loaded as input. Filters were probed with anti-ATM, anti-NBN, and anti-Hsp90α antibodies. Tubulin and total IgG levels were used as loading control for input and immunoprecipitates, respectively. Blots presented are exemplificative of at least two independent experiments. (E) Graphs represent the fold induction of ATM and NBN levels immunoprecipitated with Hsp90α in treated versus untreated cells, normalized to IgG ± SD (Student's *t*-test, $*P < 0.05$ and $***P < 0.001$, with respect to the relative control; a.d.u., arbitrary densitometric unit), derived from two independent experiments.

Hsp90α was phosphorylated at the Thr5/7 residues both in untreated and irradiated cells (see Fig. 2A), the half-time of the IR-induced phThr5/7-Hsp90α foci formation was much higher than that of γ-H2AX and 53BP1 (Fig. 4A). In fact, double immunofluorescence staining showed that phThr5/7-Hsp90α was diffusely distributed within the nuclei after 0.5 h from the exposure to 5 Gy of X-rays, small foci being fairly visible after 3 and 6 h although only partially colocalizing with γ-H2AX at 3 h from IR (10% of cells with partially colocalizing foci, on a total number of 100 cells counted; Fig. 4A), and not colocalizing with 53BP1 (Fig. 4B) and phSer343-NBN foci (Fig. 4C). However, we observed that Hsp90α failed to co-immunoprecipitate with γ-H2AX after 3 h from the exposure to 4 Gy of X-rays, both in MRC5-SV40 and LCL (Fig. 4D). In contrast to a previous study [36], these data indicate that phThr5/7-Hsp90α is not significantly recruited at the DSBs within 6 h from the exposure to X-rays, colocalizing signals possibly being determined by the high number of small phThr5/7-Hsp90α foci visible in the nuclei of irradiated cells rather than repair foci.

Hsp90α modulates the NBN-dependent MRE11 and RAD50 nuclear localization and the DDR signaling

Given the central role played by NBN in promoting the nuclear localization of MRE11 and RAD50 to allow the MRN complex formation required for the

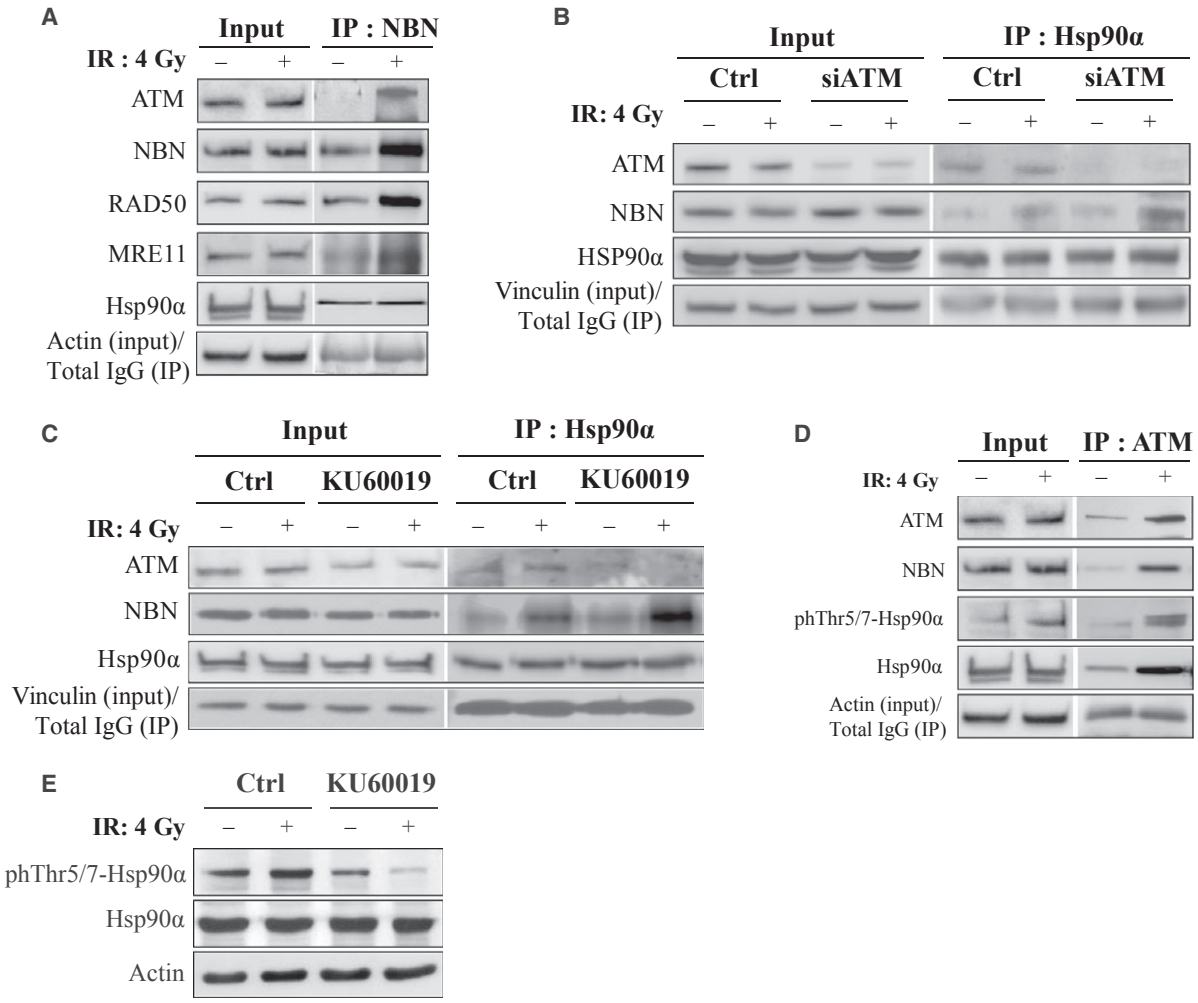

Fig. 3. The interaction between Hsp90α and NBN is regulated by ATM kinase activity. Cells were irradiated with 4 Gy of X-rays and lysed after 0.5 h. (A) MRC5-SV40 cells were immunoprecipitated using an anti-NBN an antibody. Before irradiation, (B) ATM-silenced MRC5-SV40 cells (siATM) and (C) MRC5-SV40 cells treated for 16 h with 1 μM of the ATM kinase inhibitor KU60019 were immunoprecipitated using an anti-Hsp90α antibody. (D) MRC5-SV40 cells were immunoprecipitated using an anti-ATM antibody. For IP experiments, 500 μg of total protein extracts were used, and 10 μg of total protein lysate were loaded as input. Vinculin or actin and total IgG levels were used as loading controls for input and immunoprecipitates, respectively. (E) Before irradiation, MRC5-SV40 cells were treated for 16 h with 1 μM KU60019 or with the vehicle. Filters were probed with the indicated antibodies. All the blots presented are exemplificative of at least two independent experiments.

DDR [48], we evaluated the subcellular localization of MRE11 and RAD50 in MRC5-SV40 cells treated with 1 μM 17-AAG for 8 h, then irradiated with 5 Gy of X-rays, and finally fixed after 3 h. Double immunofluorescence staining of NBN and MRE11 (Fig. 5A) or NBN and RAD50 (Fig. 5B) showed that in 17-AAG-untreated cells NBN, MRE11, and RAD50 were diffused within the nuclei and were also localized in the cytosol. After 3 h from IR, the MRN complex localized within the nuclei forming visible colocalizing foci. On the contrary, the treatment with 17-AAG, besides causing a reduced nuclear signal corresponding to NBN, affected the nuclear localization of both MRE11 and RAD50 following irradiation, the signal of both proteins remaining also strongly citoplasmatic as in controls (Fig. 5A,B).

Next, we evaluated the effect of Hsp90α inhibition on the DSBs signaling. In particular, we analyzed the effects of Hsp90α inhibition on the IR-induced activation of three members of the PIKK family (i.e., ATM, ATR, and DNA-PK). As expected, MRC5-SV40 cells treated with 1 μM 17-AAG and irradiated with 5 Gy of X-rays were characterized by reduced levels of total ATM and ATR, as well as of

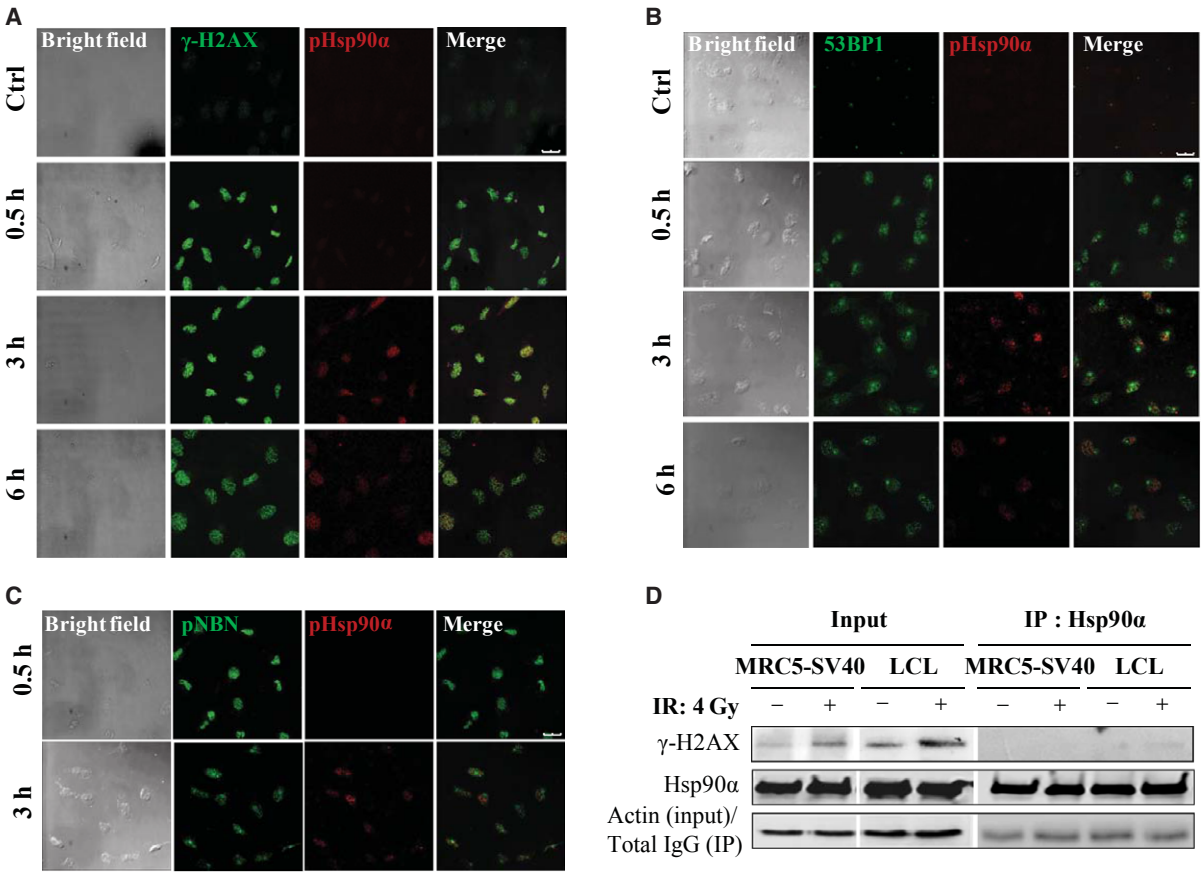

Fig. 4. The phThr5/7-Hsp90α is not recruited at the IR-induced DSBs. MRC5-SV40 cells were irradiated with 5 Gy of X-rays and fixed at the indicated time points. (A) Representative images of γ-H2AX (Alexa Fluor 488, green fluorophore) and phThr5/7-Hsp90α (pHsp90α; Alexa Fluor 610, red fluorophore) foci formation (cell image, bright field; magnification ×88; scale bar: 25 μm). (B) Representative images of 53BP1 (Alexa Fluor 488, green fluorophore) and phThr5/7-Hsp90α (pHsp90α; Alexa Fluor 610, red fluorophore) foci formation (cell image, bright field; magnification ×88; scale bar: 25 μm). (C) Representative images of phSer343-NBN (pNBN; Alexa Fluor 488, green fluorophore) and phThr5/7-Hsp90α (pHsp90α; Alexa Fluor 610, red fluorophore) foci formation (cell image, bright field; magnification ×88; scale bar: 25 μm). (D) MRC5-SV40 and LCL cells were irradiated with 4 Gy of X-rays and lysed after 3 h. Five hundred micrograms of total protein extracts were immunoprecipitated with an anti-Hsp90α an antibody and 10 μg of total protein lysate were loaded as input. Filters were checked with anti-γ-H2AX and anti-Hsp90α antibodies. Actin and total IgG levels were used as loading controls for input and immunoprecipitates, respectively. Blots presented are exemplificative of two independent experiments.

phSer1981-ATM and phSer428-ATR, compared to 17-AAG-untreated and irradiated cells (Fig. 5C). Of note, while ATM autophosphorylated at the Ser1981 residue following IR-induced DSBs [49], the Ser428 residue of ATR appeared to be phosphorylated by the CDK1 kinase in response to DNA damage *in vitro*, this phosphorylation being required for the DDR activation [50]. The treatment with 17-AAG did not alter the total levels of the DNA-PK and its phosphorylation at the Ser2056 residue after 0.5 h from irradiation, although in 17-AAG-treated cells the phosphorylation levels remained high up to 2 h from IR. As the phosphorylation of Hsp90α at the Thr5/7 residues was observed both in the absence and presence of IR-induced damage, results support the notion that besides ATM also DNA-PK phosphorylates Hsp90α [36,51], ATM, ATR, and DNA-PK sharing overlapping substrate specificities [4].

We next evaluated the effects of Hsp90α ATPase inhibition on the IR-induced phosphorylation kinetics of DDR proteins required for the DSBs repair. Consistently with the 17-AAG-dependent degradation of ATM and NBN, we observed that NBN, BRCA1 and CHK2 failed to be phosphorylated and RAD51 failed to be induced after 0.5 and 2 h from IR in 17-AAG-treated cells compared to 17-AAG-untreated and irradiated cells, in which BRCA1 and CHK2 were rapidly phosphorylated within 0.5 h from IR (Fig. 5C).

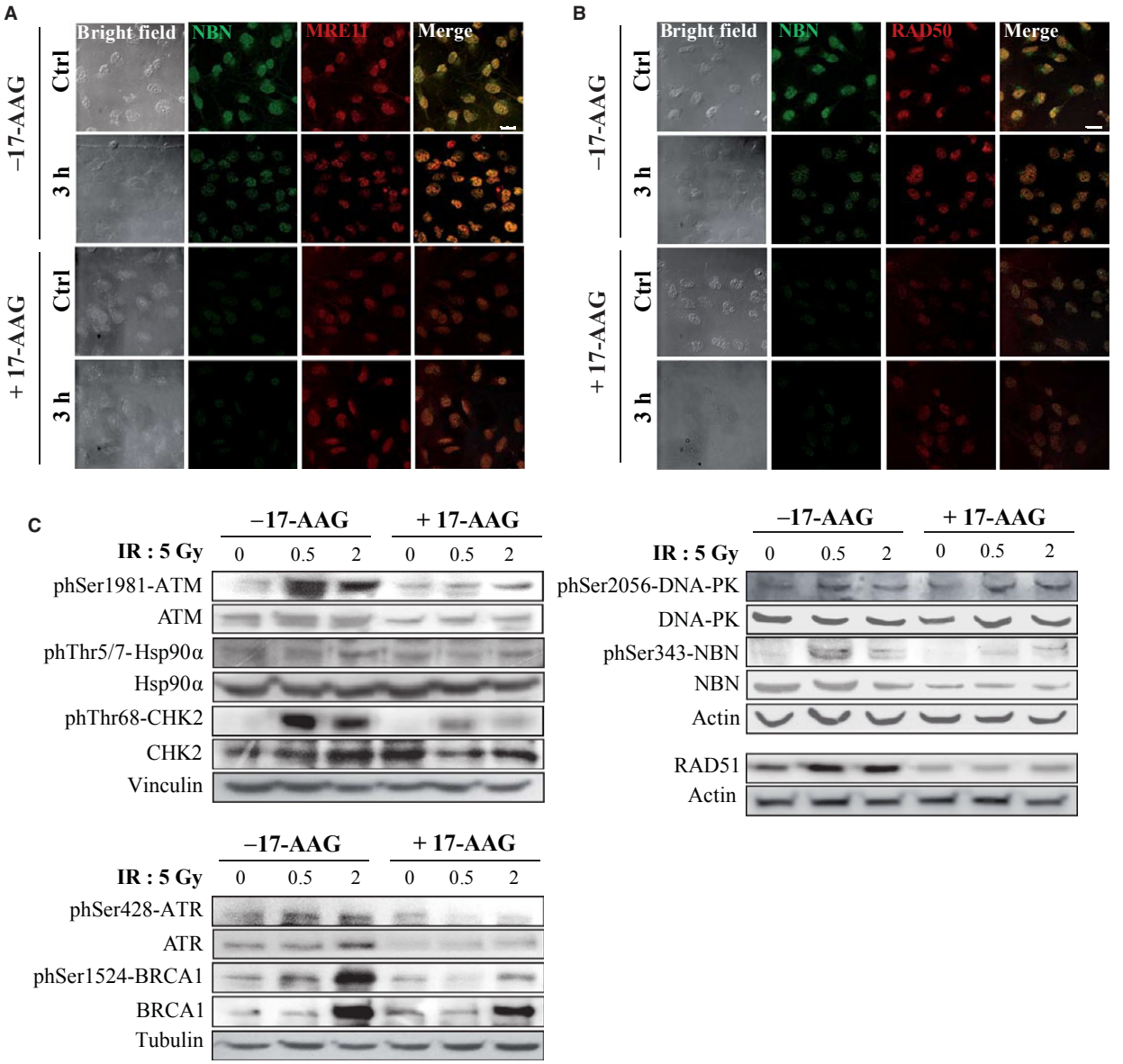

Fig. 5. Hsp90α inhibition affects the NBN-dependent MRE11 and RAD50 nuclear localization and impairs the DDR signaling. Representative images of (A) NBN (Alexa Fluor 488, green fluorophore) and MRE11 (Alexa Fluor 610, red fluorophore) foci formation and (B) NBN (Alexa Fluor 488, green fluorophore) and RAD50 (Alexa Fluor 610, red fluorophore) foci formation in MRC5-SV40 cells untreated (– 17-AAG) or exposed to 1 μM 17-AAG for 8 h (+ 17-AAG), irradiated with 5 Gy of X-rays, and fixed after 3 h (cell image, bright field; confocal microscopy images, magnification ×88; scale bar: 25 μm). (C) MRC5-SV40 cells were treated with 1 μM 17-AAG for 8 h, then irradiated with 5 Gy of X-rays, and finally harvested after 0.5 and 2 h. Ten micrograms of total protein lysates were used to perform immunoblot experiments; filters were blotted against all the indicated antibodies. The expression levels of actin, tubulin, and vinculin served as loading controls. All the blots presented are exemplificative of two independent experiments.

Hsp90α inhibition by 17-AAG causes high levels of basal and IR-induced DSBs

Although we observed that phThr5/7-Hsp90 was not recruited at the DSBs, we aimed at investigating the role of Hsp90α in the DSBs sensing and repair. To pursue this issue, the levels of γ-H2AX protein were analyzed by immunoblotting. We observed that cells treated with 17-AAG showed higher basal levels of γ-H2AX compared to 17-AAG-untreated cells, the levels of γ-H2AX remaining very high after 0.5 and 2 h from the exposure to 5 Gy of X-rays in 17-AAG-treated cells (Fig. 6A).

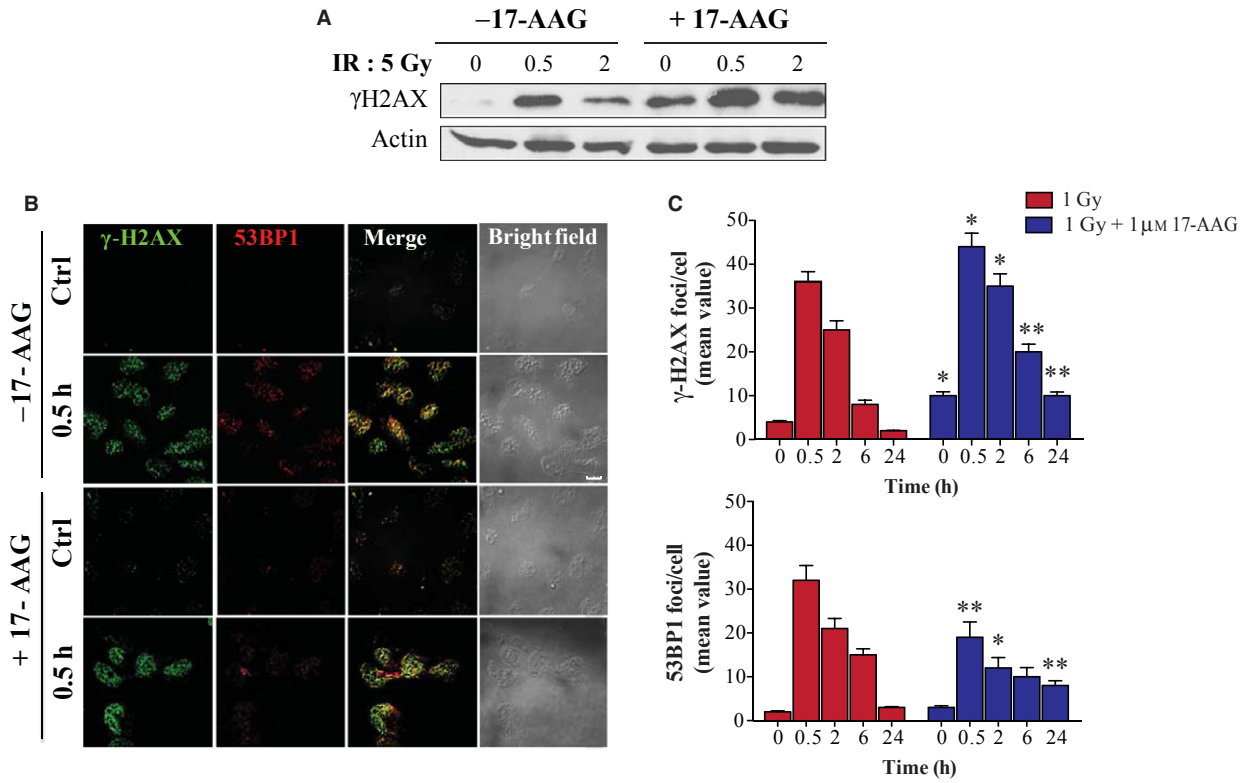

Fig. 6. Hsp90α inhibition causes high levels of basal and IR-induced DSBs. (A) MRC5-SV40 cells were treated with 1 μM 17-AAG for 8 h, then irradiated with 5 Gy of X-rays, and finally harvested after 0.5 and 2 h. Ten micrograms of total protein lysates were used to perform immunoblot experiments; filters were blotted with the anti-γ-H2AX antibody and actin was used as loading control. (B) DSBs repair kinetics evaluated by double immunofluorescence experimens. Representative images of γ-H2AX (Alexa Fluor 488, green fluorophore) and 53BP1 (Alexa Fluor 610, red fluorophore) foci formation in MRC5-SV40 cells untreated (– 17-AAG) or exposed to 1 μM 17-AAG for 8 h (+ 17-AAG), and then irradiated with 1 Gy of X-rays and fixed after 0.5 h (cell image, bright field; confocal microscopy images, magnification ×88; scale bar: 25-μm). (C) Quantitation of γ-H2AX and 53BP1 foci/cell in cells either untreated or exposed to 1 μM 17-AAG for 8 h, then irradiated with 1 Gy of X-rays, and fixed after 0.5, 2, 6, and 24 h. Graphs express the mean number of foci/cell derived from the analysis of 100 cells/experimental point, in three independent experiments ± SD (Student's *t*-test, $*P < 0.05$ and $**P < 0.01$ indicate significant differences with respect to the corresponding untreated and irradiated samples not exposed to 1 μM 17-AAG).

The double immunofluorescence staining with anti-γ-H2AX and anti-53BP1 antibodies confirmed that the inhibition of Hsp90α induced a higher number of γ-H2AX foci compared to 17-AAG-untreated MRC5-SV40 cells, while it did not influence the basal number of 53BP1 foci (Fig. 6B). Moreover, the inhibition of Hsp90α by 17-AAG caused a significant slowing down of H2AX dephosphorylation kinetics and a significant reduction in 53BP1 recruitment at the DSBs following cells exposure to 1 Gy of X-rays (Fig. 6B, C). Indeed, the mean number of γ-H2AX foci/cell in 100 cells/experimental point was significantly higher in control and irradiated 17-AAG-treated cells compared to control and irradiated 17-AAG-untreated cells, at all the time points analyzed (i.e., 0.5, 2, 6, and 24 h). On the contrary, the mean number of 53BP1 foci/cell in 100 cells/experimental point was significantly lower in the 17-AAG-treated cells than in untreated ones, at all the time points analyzed. The quantitation of the mean number of both γ-H2AX and 53BP1 foci indicated a residual damage after 24 h from IR in 17-AAG-treated cells ($P < 0.01$; Fig. 6C).

Hsp90α inhibition is known to affect cell cycle distribution [52,53]. Therefore, we wonder whether the high levels of H2AX phosphorylation caused by Hsp90α inhibition may be related to an effect of the 17-AAG treatment on the cell cycle distribution. To pursue this issue, MRC5 primary fibroblast were treated with 1 μM 17-AAG for 8 h either at a subconfluent or confluent stage, and a biparametric analysis was performed (Fig. 7). The cell cycle profiles showed that in subconfluent MRC5 primary cells, as well as in MRC5-SV40 cells (data not shown), 17-AAG caused a

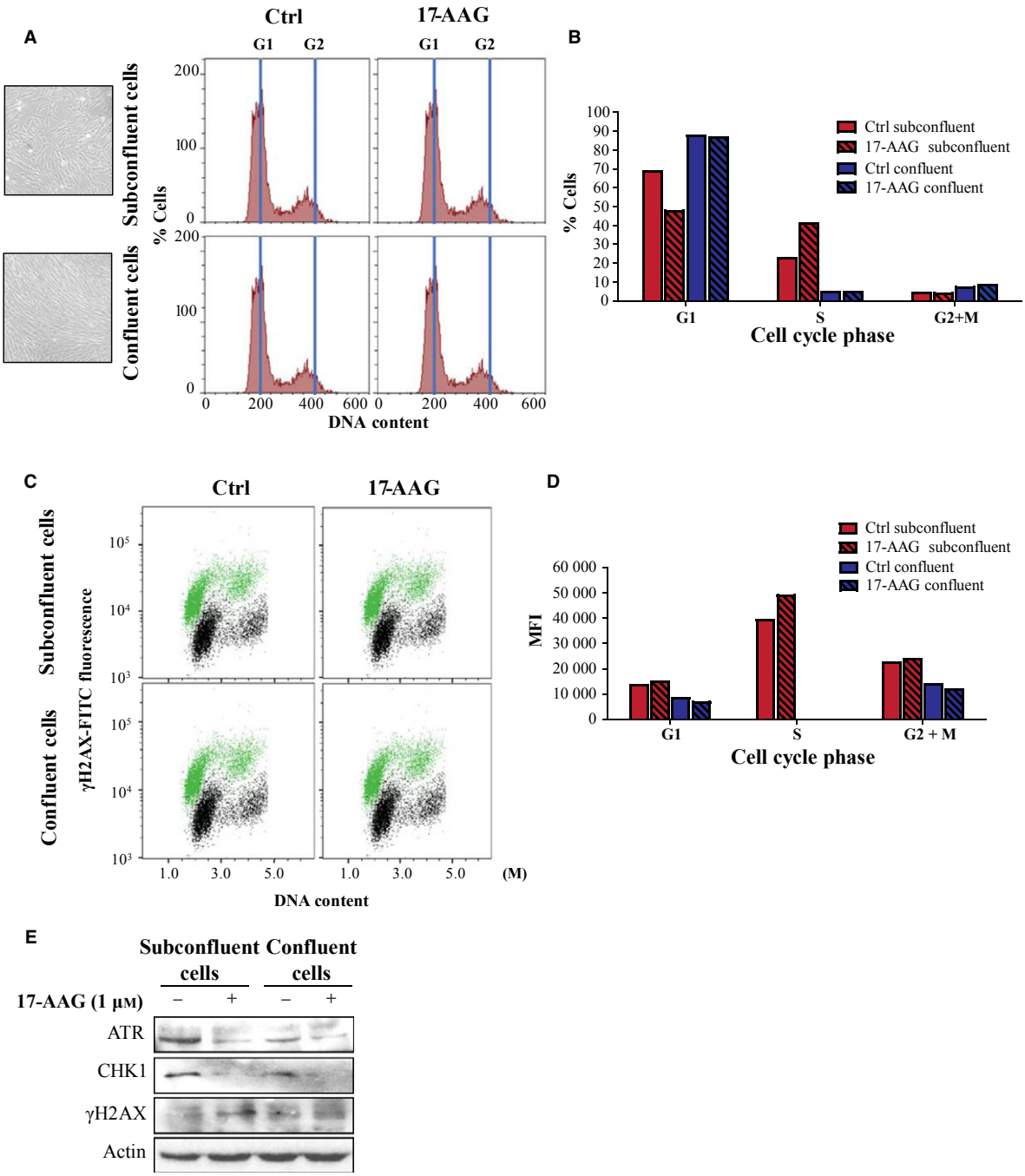

Fig. 7. The 17-AAG-induced H2AX phosphorylation arises during the S-phase of the cell cycle in proliferating cells. (A) Cell cycle profile of subconfluent and confluent primary MRC5 cells, untreated or treated with 1 μM 17-AAG for 8 h. After treatment, cells were fixed and stained with PI solution; cell cycle analysis was carried out by flow cytometry. The blue lines used as a reference represent the modal channel of G1 and G2/M populations. (B) Cell cycle distribution of subconfluent and confluent primary MRC5 cells untreated or treated with 1 μM 17-AAG for 8 h. The percentage of cells in each phase of the cell cycle has been obtained from 20 000 total events. (C) Biparametric analysis of γ-H2AX fluorescence (green) related to the cell cycle phase in subconfluent and confluent MRC5 primary cells untreated or treated with 1 μM 17-AAG for 8 h. The black signal represents the secondary antibody auto-fluorescence signal, used as control. (D) Quantitation of γ-H2AX mean fluorescence intensity (MFI) with respect to the cell cycle phase. The MFI values were obtained from 20 000 total events. (E) Subconfluent and confluent MRC5 primary cells were treated with 1 μM 17-AAG for 8 h. Cell lysates were prepared and immunoblot analyses were carried out for ATR, CHK1, and γ-H2AX; actin levels were used as loading control.

1.4-fold decrease in the percentage of G1-phase cells and a 1.8-fold increase in the percentage of S-phase cells compared to subconfluent control cells (Fig. 7A, B). The percentage of cells in the G2/M phase was not altered by the treatment with 17-AAG (Fig. 7A, B). In this context, untreated MRC5 subconfluent cells were characterized by a high basal γ-H2AX median fluorescence intensity (MFI) value in the S-phase, indicating that the breaks marked by the phosphorylated H2AX protein are associated with cell replication. The treatment of subconfluent cells with 17-AAG caused a 1.3-fold increase in the γ-H2AX MFI value in S-phase cells compared to untreated cells (Fig. 7C,D). When we analyzed confluent MRC5 cells that were mainly arrested in the G1 phase (1.3- and 1.8-fold increase in control and 17-AAG-treated confluent cells compared to control and 17-AAG-treated subconfluent cells, respectively; Fig. 7B), we observed that the treatment with 17-AAG did not cause any variation in the percentage of cells in the S and G2/M phases compared to controls (Fig. 7B), the γ-H2AX MFI values in the S-phase cells being almost close to zero compared to sub-confluent cells (Fig. 7C,D). Both in subconfluent and confluent MRC5 primary cells the γ-H2AX MFI values in the G1 and G2/M phases remained unvaried following 17-AAG treatment, indicating that the increased γ-H2AX levels observed following Hsp90α inhibition might be caused by replication stress [52,53].

Hsp90α regulates the stability of both ATR [53] and CHK1 [54], which are activated when stalled replication forks result from the replication of damaged DNA [7]. To further evaluate the correlation between the cell proliferation status and the capacity of Hsp90α to induce damage, the expression levels of ATR, CHK1, and γ-H2AX were evaluated by immunoblotting in both subconfluent and confluent MRC5 primary cells. As shown in Fig. 6E, the treatment of subconfluent MRC5 primary cells with 1 μM 17-AAG caused the reduction in ATR and CHK1 levels and the increase in γ-H2AX levels compared to untreated cells. Confluent MRC5 primary cells showed reduced basal levels of ATR and CHK1 compared to subconfluent cells, and the treatment with 17-AAG did not cause any increase in γ-H2AX levels (Fig. 7E).

Discussion

The better understanding of Hsp90α clients specificity and regulation under stress conditions is relevant to identify novel-targeted approaches to prevent cancer cell proliferation. Hsp90α inhibition, by causing the degradation of its client proteins, interferes with multiple cellular signaling pathways. Indeed, targeting the heat shock response in combination with radiotherapy sensitizes cancer cells to the IR-induced cell death [55]. In particular, quantitative phospho-proteome analyses revealed that proteins involved in the DDR, and particularly kinases, are the most susceptible targets of Hsp90α inhibition [56]. Although the interaction between Hsp90α and some DDR proteins (e.g., ATR, BRCA1, BRCA2, CHK1, the MRN complex, and RAD51) has been reported (see refs in [29]), the role of Hsp90α in the DSBs repair is still unclear. Both ATM and the MRN complex seem to depend somehow on Hsp90α, although it is controversially discussed whether ATM requires Hsp90α for its stability and/or activation via the MRN complex-dependent phosphorylation [37,53]. Here, we show that both ATM and NBN are Hsp90α clients and form a complex with the chaperone both in unstressed and irradiated cells. Indeed, the inhibition of Hsp90α activity by 17-AAG, a competitive inhibitor of ATP binding to Hsp90α that prevents its clamping around a client protein [29,38], causes the ubiquitin-mediated proteasomal degradation of ATM and NBN, affects the DDR signaling, and impairs DSBs repair. Moreover, Hsp90α inhibition induces DNA damage in proliferating cells, possibly indicating replication stress events.

According to previous data obtained in our laboratory [41], we observed that Hsp90α interacts with NBN in unstressed cells, the Hsp90α-NBN complex levels increasing at 0.5 h and returning to basal levels at 3 h from IR-induced DSBs. This indicates that Hsp90α and NBN form a complex in which Hsp90α may act as a reservoir of NBN molecules allowing their stabilization, availability, and functions during the first phases of the DDR. Upon DSBs induction, the MRN complex senses the breaks and promotes ATM autophosphorylation at the Ser1981 residue, which in turn phosphorylates NBN at the Ser343 residue [16,24,25]. Our data indicate that Hsp90α does not interact with the phosphorylated form of NBN. In fact, either the ectopic expression of a mutant NBN protein lacking the Ser343 residue phosphorylated by ATM or the lack of ATM expression or the inhibition of its kinase activity by the KU60019 inhibitor causes a marked increase in Hsp90α-NBN complex following IR, compared to cells expressing the wild-type NBN or physiological levels of the ATM kinase. Our results indicate also the existence of an Hsp90α-ATM complex in which Hsp90α acts as a reservoir of ATM and phSer1981-ATM, both in unstressed and irradiated cells. Also Hsp90α-ATM and Hsp90α-phSer1981-

ATM complex levels increase at 0.5 and 3 h from IR, phSer1981-ATM coprecipitating with Hsp90α until 6 h from IR. It can be speculated that following IR-induced DSBs, a fraction of the phosphorylated ATM dissociates from Hsp90α and re-localizes at the damaged sites, whereas a part remains in complex with the chaperone possibly allowing the phosphorylation of further nuclear substrates. Of note, Hsp90α and ATM have been described to form a complex also with the human epidermal growth factor receptor 2 (HER2), in which the inhibition of the ATM kinase activity regulates the dissociation of HER2 from Hsp90α [57]. The existence of the Hsp90α-ATM and Hsp90α-NBN complexes in unstressed cells allows the maintenance of ATM and NBN stability that is required for the rapid ATM-dependent phosphorylation of NBN in response to DNA damage. In the presence of DSBs, NBN shuttles from a complex with Hsp90α to a complex with ATM, whose kinase activity regulates NBN dissociation from Hsp90α. This allows NBN relocalization at the DSBs together with MRE11 and RAD50, where it promotes the activation of further ATM molecules [28,58,59] (Fig. 8). The treatment with 17-AAG, by causing NBN degradation and affecting the nuclear translocation of MRE11 and RAD50, impairs the signal required for the proper and rapid DSBs sensing, as demonstrated by the delayed recruitment of 53BP1 at the damaged sites.

According to a previous report [45], we observed that ATM phosphorylates Hsp90α at the Thr5 and Thr7 residues following IR. However, Hsp90α phosphorylation was still visible in cells treated with 17-AAG, possibly thanks to the kinase activity of DNA-PK [36,51]. This is in line with our data reporting that DNA-PK activity is not affected by the treatment with 17-AAG and supports the notion that redundant Hsp90α phosphorylation mechanisms may exist thanks to the overlapping substrate specificities of ATM, ATR, and DNA-PK, the source of the stimuli or of the DNA damage being determinant in the activation of a specific kinase [4].

Although it has been previously reported that phThr5/7-Hsp90α forms foci colocalizing with γ-H2AX within 3 h from the DSBs induction [36], here we have observed a very mild colocalization of phThr5/7-Hsp90α with γ-H2AX after 3 h from IR, and a complete lack of colocalization with 53BP1 foci after 0.5, 3, and 6 h from IR. The very high number of small phThr5/7-Hsp90α foci visible in the nuclei of irradiated cells and the colocalization of phThr5/7-Hsp90α with γ-H2AX only in 10% of the total cells counted, suggest that phThr5/7-Hsp90α foci do not correspond to DSB sites. The discrepancy with previous published results [36] may be ascribed to the different source and dose of irradiation used, which may influence the kinetics of phThr5/7-Hsp90α foci formation as well as their dimension. Moreover, Hsp90α does not co-immunoprecipitate with γ-H2AX following DSBs induction. Overall, the fact that Hsp90α is phosphorylated in untreated cells (present data and [36]) and does not fully localize at the IR-induced DSBs supports the hypothesis that this redundantly regulated post-translational modification (PTM) involving the ATPase region of Hsp90α is not required for the DDR but rather regulates the role of Hsp90α as a proteostasis hub, being required for the recognition of specific clients within the nucleus.

Hsp90α regulates also 53BP1 recruitment at the DSBs. We showed that in 17-AAG-treated cells the mean number of IR-induced 53BP1 foci is significantly lower compared to 17-AAG-untreated and irradiated cells, suggesting a defective recruitment of 53BP1 at the DSBs, as also reported in cells treated with AUY922, a further Hsp90α inhibitor [53]. Besides ATM and NBN, other important proteins involved in

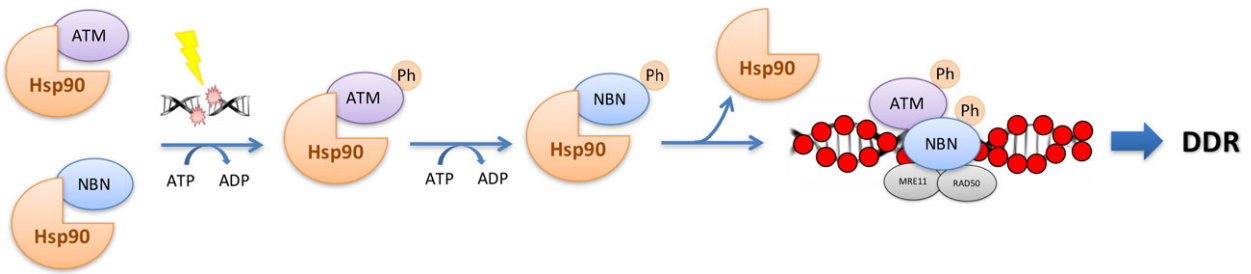

Fig. 8. Proposed model depicting the interplay between Hsp90α, ATM, and NBN. Hsp90α-ATM and Hsp90α-NBN form two complexes in unstressed cells. Upon IR-induced DSBs, ATM becomes phosphorylated and active, and in turn it rapidly phosphorylates NBN and Hsp90α molecules present within the nucleus. The phSer343-NBN form dissociates from Hsp90α and relocalizes to the DSBs together with MRE11 and RAD50, where it promotes the DDR.

the early phases of the DNA sensing, as the RING finger E3 ubiquitin ligases RNF8 and RNF168, may be dependent upon Hsp90α activity. Indeed, RNF8 and RNF168 triggers 53BP1 recruitment to DNA damage sites by regulating the degradation of the histone demethylase KDM4A-B [60], which is also regulated by the Hsp90α activity [61]. Of note, RNF8 ubiquitinates NBN at DSBs, this PTM being required for promoting stable NBN interactions with DSBs and to allow DNA repair by HR [62]. So, Hsp90α indirectly regulates 53BP1 recruitment at the DSBs, although not influencing its stability.

Therefore, Hsp90α appears to play a regulatory role on the stability of the DDR proteins rather than having a direct role in the DSBs repair. After sensing the damage, IR-induced DSBs trigger a myriad of PTMs depending on PIKK activity. These PTMs modulate the catalytic activities of many enzymes and the specificity of protein–protein and protein–DNA interactions [5]. The inhibition of Hsp90α ATPase activity, by causing the degradation of the sensing proteins ATM and NBN, affects the DSBs sensing, signaling and repair as demonstrated by: (a) the defective nuclear localization of MRE11 and RAD50, which are required for the proper DSBs sensing together with NBN; (b) the defective phosphorylation of the Ser1524 residue of BRCA1 and of the Thr68 residue of CHK2, (c) the down-regulation of the DSBs repair protein RAD51 (data here reported and [1]), (d) the DSBs repair slowdown, as marked by the kinetics of γ-H2AX de-phosphorylation and 53BP1 recruitment and disappearance, and (e) the persistence of a high number of γ-H2AX and 53BP1 foci after 24 h from IR. Since ATM and NBN cooperation is crucial for the rapid activation of CHK2 checkpoint kinase in response to IR-induced DNA damage [20,26,63], our data indicate that Hsp90α acts upstream of the ATM-NBN-CHK2 signaling axis, regulating its function(s). This model is supported by previous data reporting that 17-DMAG, a further ATPase inhibitor of Hsp90α ([29]), although not causing ATM and NBN degradation, induces a marked reduction in the amount of Hsp90α and ATM coprecipitating with NBN and of NBN coprecipitating with ATM [37].

Hsp90α inhibition causes DNA damage [36,37], as revealed by the high levels of γ-H2AX protein and by the high number of γ-H2AX and 53BP1 foci detected in 17-AAG-treated cells. The biparametric analysis of H2AX phosphorylation revealed that Hsp90α inhibition induces high levels of γ-H2AX only in highly proliferating MRC5 primary cells, in which 17-AAG causes an increase in the percentage of S-phase cells. The fact that H2AX phosphorylation has not been observed in G1 resting cells, leads to hypothesize that Hsp90α inhibition causes DNA damage in S-phase cells. Therefore, the increased γ-H2AX levels induced by 17-AAG may represent DNA breaks arising from replication stress, as a consequence of the 17-AAG-dependent degradation of ATR and CHK1, similarly to the AUY922 Hsp90α inhibitor [53]. Indeed, ATR is essential for the viability of replicating human and mouse cells since it is required to resolve stalled replication forks that form during the replication of damaged DNA [7]. Since we observed that Hsp90α inhibition by 17-AAG causes the degradation of ATM and ATR but does not affect DNA-PK levels and its phosphorylation following IR-induced damage, we suggest that this kinase is responsible for the observed H2AX phosphorylation (present data and [64]). It has been reported that besides H2AX phosphorylation, also the recruitment of several proteins forming DSB foci (e.g., 53BP1, MRN, and BRCA1) appears to be redundantly regulated and mediated by DNA-PK in the absence of ATM [64]. Remarkably, DNA-PK plays a key role in the NHEJ repair process that is active throughout the cell cycle, the HR-mediated DSBs repair being restricted to the late S and G2 phases of the cell cycle [46].

Overall, our data indicate that the Hsp90α-dependent regulation of ATM-NBN-CHK2 and ATR-CHK1 axes strongly influences cells capability to face the DNA damage. This confirms the existence of a direct link between Hsp90α functions in the nucleus and the DDR and accounts for the radiosensitizing effects of Hsp90α inhibitors. Of note, Hsp90α is spontaneously phosphorylated in various human tumors [65], but the role of its phosphorylation in the DDR remains still to be clarified.

Materials and methods

Reagents

The Hsp90α inhibitors 17-(allylamino)-17-demethoxygeldanamycin (17-AAG; Sigma-Aldrich, Saint Louis, USA) and radicicol (Sigma Aldrich) were dissolved in DMSO and ethanol, respectively, at the stock concentration of 1 mM. The 26S proteasome inhibitor carbobenzoxy-L-leucyl-L-leucyl-L-leucinal (MG-132; Calbiochem, San Diego, CA, USA) was dissolved in DMSO at the stock concentration of 50 mM. The ATM inhibitor KU60019 (Sigma Aldrich) was dissolved in DMSO at the stock concentration of 10 mM. The oligonucleotide sequence for ATM silencing (Mission® esiRNA oligos; Sigma Aldrich) was dissolved in deionized sterile water at the stock concentration of 0.02 mM.

Bradford protein assay was from Bio-Rad (Hercules, CA, USA). Protein A-Agarose and protein G PLUS-Agarose were purchased from Santa Cruz Biotechnology (Santa Cruz, CA, USA). Anti-actin antibody was from Sigma Aldrich. Anti-ATM, anti-ATR, anti-CHK2, anti-γ-H2AX, anti-Hsp90α, anti-MRE11, anti-RAD50, anti-RAD51, anti-ubiquitin, and anti-vinculin antibodies were from Santa Cruz Biotechnology. Anti-pSer1981-ATM, anti-pSer428-ATR, anti-pSer1524-BRCA1, anti-pThr68-CHK2, anti-pThr5/7-Hsp90α antibodies were from Cell Signaling Technology (Danvers, MA, USA). Anti-DNA-PK, anti-pSer2056-DNA-PK, anti-CHK1, and anti-BRCA1 antibodies were purchased from Abcam (Cambridge, UK). Anti-NBN antibody was from GeneTex (Alton Pkwy Irvine, CA, USA). Anti-53BP1 and anti-γ-H2AX were from Millipore (Billerica, MA, USA). The Alexa Fluor 488-conjugated goat anti-(mouse IgG) and Alexa Fluor 610-conjugated goat anti-rabbit antibodies were from Immunological Sciences (Rome, Italy). The HRP-conjugated secondary antibodies and chemiluminescence reagent were from Bio-Rad.

Cell lines and culture conditions

Adherent cells [i.e., SV40-immortalized MRC5 cells (here named MRC5-SV40); MRC5 primary cells; SV40-immortalized fibroblasts established from a patient affected by NBS (OMIM #2512609), homozygous for the 657del5 mutation in the *NBN* gene (here named $NBN^{657del5}$; [66]); NBS-derived cells carrying the point mutation Ser343Ala at the ATM phosphorylation site within NBN (here named 343S, kindly provided by K. Komatsu); [67]] were grown in Dulbecco Modified Eagle's medium (DMEM; Biowest, Nuaillé, France) supplemented with 10% FBS (Corning, NY, USA), 2 mM L-glutamine (Biowest), 100 $mg{\cdot}mL^{-1}$ penicillin, and 100 $mg{\cdot}mL^{-1}$ streptomycin (Sigma Aldrich). Cells established from a normal donor (here named LCL) and from a patient affected by ataxia-telangiectasia (OMIM #208900; here named $ATM^{-/-}$; [68]) were maintained in RPMI 1640 medium (GIBCO Life Technologies, Monza, Italy) supplemented with 10% heat-inactivated FBS, 2 mM L-glutamine, 100 $mg{\cdot}mL^{-1}$ penicillin, and 100 $mg{\cdot}mL^{-1}$ streptomycin. In all the experiments in which cells were treated with 17-AAG and/or MG-132, DMSO was used as a control vehicle (final concentration 1%).

Ionizing radiation treatment

Cells were irradiated with a dose of 1–5 Gy depending on the endpoint analyzed, using a MGL 300/6-D X-ray apparatus (Gilardoni S.P.A., Mandello del Lario (LC), Italy; 250 kV, 6 mA, Cu filter) operating at a dose rate of 0.53 $Gy{\cdot}min^{-1}$. Cells were harvested after IR according to the experimental plan.

siRNA transfection

The transient silencing of ATM in MRC5-SV40 cells was performed by double transfection [69] using 5 nM of siRNA and Lipofectamine RNAiMAX transfection reagent (Invitrogen, Waltham, MA, USA), according to the manufacturer's instructions. Control cells were transfected with the Mission® siRNA Universal Negative Controls, using the same amount of the transfection medium. Cells were analyzed 48 h after the second transfection by immunoblot experiments.

Immunoprecipitation

Cells were lysed using the NP-40 lysis buffer (20 mM Tris-HCl pH 8.0, 137 mM NaCl, 10% glycerol (v/v), 1% NP-40 (v/v), 10 mM EDTA, 1 $mg{\cdot}mL^{-1}$ aprotinin, 1 $mg{\cdot}mL^{-1}$ leupeptin, 1 $mg{\cdot}mL^{-1}$ pepstatin, 1 mM orthovanadate, and 2 mM PMSF). Five hundred micrograms of whole cell lysates were precleared using 30 μL of protein A-agarose or protein G PLUS-agarose beads for 1 h at 4 °C, and then incubated with the primary antibody for 4 h at 4 °C. Finally, 30 μL of protein A-agarose or protein G PLUS-agarose beads were added to the mixture and incubated over night (ON) at 4 °C. Immunoprecipitates were washed with lysis buffer and loaded on an SDS/PAGE. Experiments were repeated at least three times.

Western blot

Proteins were loaded on an SDS/PAGE and transferred on a polyvinylidene fluoride (PVDF) membrane (Bio-Rad). Membranes were blocked for 1 h at room temperature (RT) with either 3% BSA/PBS (w/v) or 0.1% Tween-20 (v/v) or with 3% nonfat dry milk/PBS (w/v) and 0.1% Tween-20 (v/v), and then incubated with primary antibodies for either 2 h at RT or ON at 4 °C. Finally, membranes were incubated for 1 h at RT with the secondary antibodies. Proteins were visualized by the enhanced chemiluminescence detection system. Experiments were repeated at least three times.

Immunofluorescence

Cells were fixed in 4% paraformaldehyde (w/v) for 10 min on ice. After permeabilization with PBS/0.2% Triton X-100 (v/v), cells were blocked in 10% BSA/PBS (w/v) for 1 h at RT. Following incubation with primary antibodies diluted in 1% BSA/PBS ON at 4 °C, slides were incubated for 1 h at 37 °C with 10 $\mu g{\cdot}mL^{-1}$ of secondary antibodies. Confocal analysis was performed using the LCS Leica confocal microscope (Leica Microsystems, Heidelberg, Germany). Quantitative analysis was carried out by counting foci in 100 cells/experimental point, in three independent experiments.

MTT assay

MRC5-SV40 cells were seeded in 96-well plates at a concentration of 1×10^5 cells per well. After 24 h, the cell monolayers were exposed to either DMSO or 0.125, 0.25, 0.5, 1 μM 17-AAG for 24, 48 and 72 h. A MTT solution (stock solution of 0.5 mg·mL^{-1}) was then added to the cell culture and incubated for 2.5 h at 37 °C. Formazan crystals were then dissolved in lysis buffer (4 mM HCl, 0.1% NP40 (v/v) in isopropanol). The plates were analyzed using a microplate reader at 570 nm (BioTek ELx800 Absorbance Microplate Reader, Winooski, VT, USA). As controls, untreated cultures were performed under identical conditions.

Flow cytometric analysis of γ-H2AX and cell cycle analysis

The MRC5 primary cells were treated with 1 μM 17-AAG for 8 h and next 1×10^6 cells were fixed on ice for 15 min with PBS/1% paraformaldehyde (w/v), washed with PBS, permeabilized with ice-cold 70%, and stored for 24 h at −20 °C. After rehydration with PBS/0.2% Triton X-100 (v/v)/1% BSA (w/v), cells were incubated for 2 h at 37 °C with anti-γ-H2AX antibody and for 1 h at 37 °C with the anti-mouse Alexa488-conjugated secondary antibody. After that, cells were resuspended in PBS containing 0.18 mg·mL^{-1} propidium iodide (PI; Sigma) and 0.4 mg·mL^{-1} DNase-free RNase (type 1-A; Sigma Aldrich), incubated for 0.5 h at 37 °C, and analyzed. To better define the fluorescence due to the phosphorylation of H2AX related to the cell cycle phases, three electronic polygonal gates were designed on G1/G0, S and G2/M in biparametric DNA content/γ-H2AX dot plot, and a mean fluorescence intensity (MFI) was measured in each of them. The analyses were performed on 20 000 total events (CytoFLEX Beckman Coulter, Brea, CA, USA), and data were analyzed using the CYTEXPERT Software (version 1.2; Beckman Coulter).

Statistical analysis

Densitometric analyses were performed using the freeware software IMAGEJ (https://imagej.nih.gov/ij) by quantifying the band intensity of the protein of interest with respect to the relative loading control band (i.e., vinculin, actin, or total IgG) intensity. Data were expressed as mean values ± standard deviation (SD). Statistical analysis was performed using the Student's *t*-test. The P values < 0.05 were considered significant and the P values < 0.01 were assigned highly significant.

Acknowledegements

We are grateful to Dr. Ilio Vitale (Università di Tor Vergata, Roma, Italy) for providing the KU60019 ATM inhibitor, and to Prof. Filippo Acconcia (Roma Tre University, Department of Sciences) for providing the anti-ubiquitin antibody. This work was partially supported by research funding from Roma Tre University (CLA 2015 and CLA 2016 to AdM; CLA 2015 to AA).

Conflicts of interest

No conflicts of interest to declare.

Author contributions

AA, AdM, SL, and RP conceived and designed the experiments. AdM, RP, and SL performed the experiments. AA, AdM, PA, RP, and SL analyzed the data. AdM, AA, PA, and SL contributed reagents/materials/analysis tools. AdM, AA, and RP wrote the paper.

References

1 Chapman JR, Taylor MR & Boulton SJ (2012) Playing the end game: DNA double-strand break repair pathway choice. *Mol Cell* **47**, 497–510.
2 Goodarzi AA & Jeggo PA (2013) The repair and signaling responses to DNA double-strand breaks. *Adv Genet* **82**, 1–45.
3 Mladenov E, Magin S, Soni A & Iliakis G (2016) DNA double-strand-break repair in higher eukaryotes and its role in genomic instability and cancer: cell cycle and proliferation-dependent regulation. *Semin Cancer Biol* **37–38**, 51–64.
4 Abraham RT (2004) PI 3-kinase related kinases: 'big' players in stress-induced signaling pathways. *DNA Repair (Amst)* **3**, 883–887.
5 Shiloh Y & Ziv Y (2013) The ATM protein kinase: regulating the cellular response to genotoxic stress, and more. *Nat Rev Mol Cell Biol* **14**, 197–210.
6 Shrivastav M, Miller CA, De Haro LP, Durant ST, Chen BP, Chen DJ & Nickoloff JA (2009) DNA-PKcs and ATM co-regulate DNA double-strand break repair. *DNA Repair (Amst)* **8**, 920–929.
7 Cimprich KA & Cortez D (2008) ATR: an essential regulator of genome integrity. *Nat Rev Mol Cell Biol* **9**, 616–627.
8 Yang J, Yu Y, Hamrick HE & Duerksen-Hughes PJ (2003) ATM, ATR and DNA-PK: initiators of the cellular genotoxic stress responses. *Carcinogenesis* **24**, 1571–1580.
9 Ciccia A & Elledge SJ (2010) The DNA damage response: making it safe to play with knives. *Mol Cell* **40**, 179–204.
10 Matsuoka S, Ballif BA, Smogorzewska A, McDonald ER, Hurov KE, Luo J, Bakalarski CE, Zhao Z,

Solimini N, Lerenthal Y *et al.* (2007) ATM and ATR substrate analysis reveals extensive protein networks responsive to DNA damage. *Science* **316**, 1160–1166.
11 Jowsey P, Morrice NA, Hastie CJ, McLauchlan H, Toth R & Rouse J (2007) Characterisation of the sites of DNA damage-induced 53BP1 phosphorylation catalysed by ATM and ATR. *DNA Repair (Amst)* **6**, 1536–1544.
12 Gatei M, Scott SP, Filippovitch I, Soronika N, Lavin MF, Weber B & Khanna KK (2000) Role for ATM in DNA damage-induced phosphorylation of BRCA1. *Cancer Res* **60**, 3299–3304.
13 Burma S, Chen BP, Murphy M, Kurimasa A & Chen DJ (2001) ATM phosphorylates histone H2AX in response to DNA double-strand breaks. *J Biol Chem* **276**, 42462–42467.
14 Jungmichel S, Clapperton JA, Lloyd J, Hari FJ, Spycher C, Pavic L, Li J, Haire LF, Bonalli M, Larsen DH *et al.* (2012) The molecular basis of ATM-dependent dimerization of the Mdc1 DNA damage checkpoint mediator. *Nucleic Acids Res* **40**, 3913–3928.
15 Di Virgilio M, Ying CY & Gautier J (2009) PIKK-dependent phosphorylation of Mre11 induces MRN complex inactivation by disassembly from chromatin. *DNA Repair (Amst)* **8**, 1311–1320.
16 Lim DS, Kim ST, Xu B, Maser RS, Lin J, Petrini JH & Kastan MB (2000) ATM phosphorylates p95/nbs1 in an S-phase checkpoint pathway. *Nature* **404**, 613–617.
17 Gatei M, Jakob B, Chen P, Kijas AW, Becherel OJ, Gueven N, Birrell G, Lee JH, Paull TT, Lerenthal Y *et al.* (2011) ATM protein-dependent phosphorylation of Rad50 protein regulates DNA repair and cell cycle control. *J Biol Chem* **286**, 31542–31556.
18 Siliciano JD, Canman CE, Taya Y, Sakaguchi K, Appella E & Kastan MB (1997) DNA damage induces phosphorylation of the amino terminus of p53. *Genes Dev* **11**, 3471–3481.
19 Shin MH, Yuan M, Zhang H, Margolick JB & Kai M (2012) ATM-dependent phosphorylation of the checkpoint clamp regulates repair pathways and maintains genomic stability. *Cell Cycle* **11**, 1796–1803.
20 Smith J, Tho LM, Xu N & Gillespie DA (2010) The ATM-Chk2 and ATR-Chk1 pathways in DNA damage signaling and cancer. *Adv Cancer Res* **108**, 73–112.
21 Chen BP, Uematsu N, Kobayashi J, Lerenthal Y, Krempler A, Yajima H, Lobrich M, Shiloh Y & Chen DJ (2007) Ataxia telangiectasia mutated (ATM) is essential for DNA-PKcs phosphorylations at the Thr-2609 cluster upon DNA double strand break. *J Biol Chem* **282**, 6582–6587.
22 Xu N, Lao Y, Zhang Y & Gillespie DA (2012) Akt: a double-edged sword in cell proliferation and genome stability. *J Oncol* **2012**, 951724.
23 Stracker TH & Petrini JH (2011) The MRE11 complex: starting from the ends. *Nat Rev Mol Cell Biol* **12**, 90–103.
24 Gatei M, Young D, Cerosaletti KM, Desai-Mehta A, Spring K, Kozlov S, Lavin MF, Gatti RA, Concannon P & Khanna K (2000) ATM-dependent phosphorylation of nibrin in response to radiation exposure. *Nat Genet* **25**, 115–119.
25 Wu X, Ranganathan V, Weisman DS, Heine WF, Ciccone DN, O'Neill TB, Crick KE, Pierce KA, Lane WS, Rathbun G *et al.* (2000) ATM phosphorylation of Nijmegen breakage syndrome protein is required in a DNA damage response. *Nature* **405**, 477–482.
26 Difilippantonio S & Nussenzweig A (2007) The NBS1-ATM connection revisited. *Cell Cycle* **6**, 2366–2370.
27 Stracker TH, Morales M, Couto SS, Hussein H & Petrini JH (2007) The carboxy terminus of NBS1 is required for induction of apoptosis by the MRE11 complex. *Nature* **447**, 218–221.
28 Lee JH & Paull TT (2004) Direct activation of the ATM protein kinase by the Mre11/Rad50/Nbs1 complex. *Science* **304**, 93–96.
29 Pennisi R, Ascenzi P & di Masi A (2015) Hsp90: a new player in DNA repair? *Biomolecules* **5**, 2589–2618.
30 Hartl FU, Bracher A & Hayer-Hartl M (2011) Molecular chaperones in protein folding and proteostasis. *Nature* **475**, 324–332.
31 Kim YE, Hipp MS, Bracher A, Hayer-Hartl M & Hartl FU (2013) Molecular chaperone functions in protein folding and proteostasis. *Annu Rev Biochem* **82**, 323–355.
32 Morimoto RI (2011) The heat shock response: Systems biology of proteotoxic stress in aging and disease. *Cold Spring Harb Symp Quant Biol* **76**, 91–99.
33 Taipale M, Jarosz DF & Lindquist S (2010) HSP90 at the hub of protein homeostasis: emerging mechanistic insights. *Nat Rev Mol Cell Biol* **11**, 515–528.
34 Makhnevych T & Houry WA (2012) The role of Hsp90 in protein complex assembly. *Biochim Biophys Acta* **1823**, 674–682.
35 Young JC, Moarefi I & Hartl FU (2001) Hsp90: a specialized but essential protein-folding tool. *J Cell Biol* **154**, 267–273.
36 Quanz M, Herbette A, Sayarath M, de Koning L, Dubois T, Sun JS & Dutreix M (2012) Heat shock protein 90alpha (Hsp90alpha) is phosphorylated in response to DNA damage and accumulates in repair foci. *J Biol Chem* **287**, 8803–8815.
37 Dote H, Burgan WE, Camphausen K & Tofilon PJ (2006) Inhibition of hsp90 compromises the DNA damage response to radiation. *Cancer Res* **66**, 9211–9220.
38 Jhaveri K, Taldone T, Modi S & Chiosis G (2012) Advances in the clinical development of heat shock protein 90 (Hsp90) inhibitors in cancers. *Biochim Biophys Acta* **1823**, 742–755.

39 Blagg BS & Kerr TD (2006) Hsp90 inhibitors: small molecules that transform the Hsp90 protein folding machinery into a catalyst for protein degradation. *Med Res Rev* **26**, 310–338.
40 Wang S, Wang X, Du Z, Liu Y, Huang D, Zheng K, Liu K, Zhang Y, Zhong X & Wang Y (2014) SNX-25a, a novel Hsp90 inhibitor, inhibited human cancer growth more potently than 17-AAG. *Biochem Biophys Res Commun* **450**, 73–80.
41 Cilli D, Mirasole C, Pennisi R, Pallotta V, D'Alessandro A, Antoccia A, Zolla L, Ascenzi P & di Masi A (2014) Identification of the interactors of human nibrin (NBN) and of its 26 kDa and 70 kDa fragments arising from the NBN 657del5 founder mutation. *PLoS ONE* **9**, e114651.
42 Mendez G, Cilli D, Berardinelli F, Viganotti M, Ascenzi P, Tanzarella C, Antoccia A & di Masi A (2012) Cleavage of the BRCT tandem domains of nibrin by the 657del5 mutation affects the DNA damage response less than the Arg215Trp mutation. *IUBMB Life* **64**, 853–861.
43 Kruger L, Demuth I, Neitzel H, Varon R, Sperling K, Chrzanowska KH, Seemanova E & Digweed M (2007) Cancer incidence in Nijmegen breakage syndrome is modulated by the amount of a variant NBS protein. *Carcinogenesis* **28**, 107–111.
44 Maser RS, Zinkel R & Petrini JH (2001) An alternative mode of translation permits production of a variant NBS1 protein from the common Nijmegen breakage syndrome allele. *Nat Genet* **27**, 417–421.
45 Elaimy AL, Ahsan A, Marsh K, Pratt WB, Ray D, Lawrence TS & Nyati MK (2016) ATM is the primary kinase responsible for phosphorylation of Hsp90alpha after ionizing radiation. *Oncotarget* **7**, 82450–82457.
46 Panier S & Boulton SJ (2014) Double-strand break repair: 53BP1 comes into focus. *Nat Rev Mol Cell Biol* **15**, 7–18.
47 Scully R & Xie A (2013) Double strand break repair functions of histone H2AX. *Mutat Res* **750**, 5–14.
48 Cerosaletti K & Concannon P (2004) Independent roles for nibrin and Mre11-Rad50 in the activation and function of Atm. *J Biol Chem* **279**, 38813–38819.
49 Bakkenist CJ & Kastan MB (2003) DNA damage activates ATM through intermolecular autophosphorylation and dimer dissociation. *Nature* **421**, 499–506.
50 Hilton BA, Li Z, Musich PR, Wang H, Cartwright BM, Serrano M, Zhou XZ, Lu KP & Zou Y (2015) ATR plays a direct antiapoptotic role at mitochondria, which is regulated by prolyl isomerase Pin1. *Mol Cell* **60**, 35–46.
51 Lees-Miller SP & Anderson CW (1989) The human double-stranded DNA-activated protein kinase phosphorylates the 90-kDa heat-shock protein, hsp90 alpha at two NH2-terminal threonine residues. *J Biol Chem* **264**, 17275–17280.
52 Arlander SJ, Eapen AK, Vroman BT, McDonald RJ, Toft DO & Karnitz LM (2003) Hsp90 inhibition depletes Chk1 and sensitizes tumor cells to replication stress. *J Biol Chem* **278**, 52572–52577.
53 Ha K, Fiskus W, Rao R, Balusu R, Venkannagari S, Nalabothula NR & Bhalla KN (2011) Hsp90 inhibitor-mediated disruption of chaperone association of ATR with hsp90 sensitizes cancer cells to DNA damage. *Mol Cancer Ther* **10**, 1194–1206.
54 Arlander SJ, Felts SJ, Wagner JM, Stensgard B, Toft DO & Karnitz LM (2006) Chaperoning checkpoint kinase 1 (Chk1), an Hsp90 client, with purified chaperones. *J Biol Chem* **281**, 2989–2998.
55 Lauber K, Brix N, Ernst A, Hennel R, Krombach J, Anders H & Belka C (2015) Targeting the heat shock response in combination with radiotherapy: sensitizing cancer cells to irradiation-induced cell death and heating up their immunogenicity. *Cancer Lett* **368**, 209–229.
56 Sharma K, Vabulas RM, Macek B, Pinkert S, Cox J, Mann M & Hartl FU (2012) Quantitative proteomics reveals that Hsp90 inhibition preferentially targets kinases and the DNA damage response. *Mol Cell Proteomics* **11**, M111.
57 Stagni V, Manni I, Oropallo V, Mottolese M, Di Benedetto A, Piaggio G, Falcioni R, Giaccari D, Di Carlo S, Sperati F *et al.* (2015) ATM kinase sustains HER2 tumorigenicity in breast cancer. *Nat Commun* **6**, 6886.
58 Uziel T, Lerenthal Y, Moyal L, Andegeko Y, Mittelman L & Shiloh Y (2003) Requirement of the MRN complex for ATM activation by DNA damage. *EMBO J* **22**, 5612–5621.
59 You Z, Chahwan C, Bailis J, Hunter T & Russell P (2005) ATM activation and its recruitment to damaged DNA require binding to the C terminus of Nbs1. *Mol Cell Biol* **25**, 5363–5379.
60 Mallette FA, Mattiroli F, Cui G, Young LC, Hendzel MJ, Mer G, Sixma TK & Richard S (2012) RNF8- and RNF168-dependent degradation of KDM4A/JMJD2A triggers 53BP1 recruitment to DNA damage sites. *EMBO J* **31**, 1865–1878.
61 Ipenberg I, Guttmann-Raviv N, Khoury HP, Kupershmit I & Ayoub N (2013) Heat shock protein 90 (Hsp90) selectively regulates the stability of KDM4B/JMJD2B histone demethylase. *J Biol Chem* **288**, 14681–14687.
62 Lu CS, Truong LN, Aslanian A, Shi LZ, Li Y, Hwang PY, Koh KH, Hunter T, Yates JR III, Berns MW *et al.* (2012) The RING finger protein RNF8 ubiquitinates Nbs1 to promote DNA double-strand break repair by homologous recombination. *J Biol Chem* **287**, 43984–43994.

63 Buscemi G, Savio C, Zannini L, Micciche F, Masnada D, Nakanishi M, Tauchi H, Komatsu K, Mizutani S, Khanna K *et al.* (2001) Chk2 activation dependence on Nbs1 after DNA damage. *Mol Cell Biol* **21**, 5214–5222.
64 Stiff T, O'Driscoll M, Rief N, Iwabuchi K, Lobrich M & Jeggo PA (2004) ATM and DNA-PK function redundantly to phosphorylate H2AX after exposure to ionizing radiation. *Cancer Res* **64**, 2390–2396.
65 Wang X, Song X, Zhuo W, Fu Y, Shi H, Liang Y, Tong M, Chang G & Luo Y (2009) The regulatory mechanism of Hsp90alpha secretion and its function in tumor malignancy. *Proc Natl Acad Sci USA* **106**, 21288–21293.
66 Yamazaki V, Wegner RD & Kirchgessner CU (1998) Characterization of cell cycle checkpoint responses after ionizing radiation in Nijmegen breakage syndrome cells. *Cancer Res* **58**, 2316–2322.
67 Antoccia A, Sakamoto S, Matsuura S, Tauchi H & Komatsu K (2008) NBS1 prevents chromatid-type aberrations through ATM-dependent interactions with SMC1. *Radiat Res* **170**, 345–352.
68 Antoccia A, Chessa L, Ricordy R & Tanzarella C (1995) Modulation of radiation-induced chromosomal damage by inhibitors of DNA repair and flow cytometric analysis in ataxia telangiectasia cells with 'intermediate radiosensitivity'. *Mutagenesis* **10**, 523–529.
69 Totta P, Pesiri V, Enari M, Marino M & Acconcia F (2015) Clathrin heavy chain interacts with estrogen receptor alpha and modulates 17beta-estradiol signaling. *Mol Endocrinol* **29**, 739–755.